ISBN: 978-3-95450-226-4 ISSN: 2222-5692 doi:10.18429/JACoW-ECRIS2020-TUYZO01

ADVANCEMENTS IN SELF-CONSISTENT MODELING OF TIME- AND SPACE-DEPENDENT PHENOMENA IN ECRIS PLASMA

A. Pidatella*, D. Mascali, B. Mishra, E. Naselli [1], G. Torrisi, INFN-LNS, Catania, Italy
A. Galatà, INFN-LNL, Legnaro, Italy
[1]also at Department of Physics and Astronomy, University of Catania, Italy

Abstract

The resonant interaction of electrons with the microwave radiation in Electron Cyclotron Resonance Ion Sources (ECRIS) plasma leads to a strongly anisotropic electron energy distribution function (EEDF), given as a convolution of two to three electron populations, with the anisotropy that might trigger kinetic instabilities. At the INFN, further efforts have been paid to improve and update the self-consistent 3D numerical codes for plasma electrons kinetics. Progresses have opened several perspectives. It is now possible to derive a space-resolved EEDF, providing local information on the electron properties in the plasma. Also, the code has been updated to provide reaction rates of electromagnetic emissions, including X-ray fluorescence. Estimate of local ion charge state distribution is potentially possible, and first evaluations are ongoing. Dealing with fast-transient mechanisms, such as electromagnetic emission via the electron-cyclotron MASER instability, the code is now updated for locally evaluating EEDF anisotropy. We will present the collected results, which we believe to have a relevant impact both on the ECRIS plasma physics and on the INFN's PANDORA project that plans to use ECR plasmas for fundamental studies in Nuclear and AstroNuclear Physics.

INTRODUCTION AND MOTIVATION

Electron cyclotron resonance ion sources (ECRIS) are able to produce intense and stable beams of highly charged ions, required by accelerators for nuclear and applied physics. Progress and improvements in understanding ECRIS have been made in the past years. However, they mostly consisted in increasing the power of the RF heating-wave, as well as the intensity of magnetic fields, accordingly to the "scaling laws" [1], with constraint represented by present technological limits. In view of this, a deeper knowledge of plasma confinement dynamics and parameters - electron density, temperature, and ion charge state distribution (CSD) - is highly desirable, since the properties of the extracted ion beam (in terms of intensity, average charge state and quality) strictly depend on plasma structure and properties.

ECRIS with a minimum-B magnetic field structure are conventionally employed as source of multicharged ion beams. This magnetic structure consists in a superposition of solenoid and sextupole fields, which topology leads to closed ECR surface, where wave-to-particle resonant coupling and energy transfer take place, and a sufficient plasma confinement for a step-wise ionization to high charge states is realized. However, the resulting electron energy distribution is strongly anisotropic, made at least of two to three main populations: cold (1-100 eV), warm (0.1-10 keV), and hot (10 keV - 1 MeV) electrons. Because of such anisotropic distribution, the system becomes prone to kinetic instabilities, limiting ECRIS performances. These phenomena are mainly driven by warm and hot electrons whose transverse velocity $v_\perp$ (with respect to the magnetic field) dominates over the longitudinal one $v_\parallel$ [2]. These kinetics instabilities can also leave electromagnetic signatures, consisting in powerful bursts of microwave and x-ray radiation, due to a resonant enhancement of plasma waves as an effect of non-linear interactions with hot electrons. This phenomenon is known as electron cyclotron MASER instability [3–5]. Even though many studies have been conducted, the exact mechanism of turbulent regimes of plasmas is still unknown and a deeper investigation is necessary.

The present work shows some preliminary advancements in numerical modeling and studying the aforementioned plasmas, providing space-resolved information both on typical electron energy distribution functions (EEDFs) and on a space-resolved velocity distribution of electron in unstable plasma. These numerical tools will possibly allow exploring space-dependent mechanisms, and to have a better predicting power for both space- and time-dependent phenomena in ECRIS plasma.

3D MODELING OF ECRIS PLASMA

In the case of ECR plasmas, a self-consistent approach is desirable to solve the collisional Vlasov-Boltzmann equations [6]. In this context, the INFN-LNS jointly with the INFN-LNL group, have developed an iterative routine to produce a self-consistent description of ECR *stationary* plasmas. The overall code results from a strict interplay between a kinetic code, or 'particle mover', developed in MATLAB©, and a FEM electromagnetic solver (we used COMSOL - Multiphysics©), for evaluating the electromagnetic (EM) fields once given local charge densities. A self-consistent approach is necessary since the propagating EM field affects electron motion and energy via a resonant interaction. On the other hand, the plasma - being an anisotropic and dispersive medium - presents a 3D dielectric tensor which must be in turn considered in the calculation of the EM field [7]. The 'particle mover' code solves the equations of motion of a given number of particles followed for their entire life (i.e. until they impinge on the chamber walls, meaning they have been de-confined). In this sense, our approach can be

* pidatella@lns.infn.it

ISBN: 978-3-95450-226-4 ISSN: 2222-5692 doi:10.18429/JACoW-ECRIS2020-TUYZO01

defined as a 'stationary' particle-in-cell code, describing the stationary structure of the plasma in the phase space: the local charges densities are evaluated through the 'trick' of density accumulation in a 3D grid. Particles trajectories evolve in parallel (simultaneously) and the local density accumulation is made as single particles move throughout the single cells in the volume contained inside the plasma chamber. During each i-th step of kinetic simulation, the EM field is taken as stationary and coming from the $(i-1)$-th step. The self-consistent loop is run until convergence is achieved between the $(i-1)$-th and i-th step, looking at both 3D density and EM field maps. Further details on the numerical machinery can be found in Ref. [6].

The established numerical code has many times proven its robustness and validity, for instance investigating the so-called frequency tuning effect [8], and reproducing experimental results for light- and heavy-ion dynamics in ECR-based charge breeding devices [9, 10].

SPACE-RESOLVED ELECTRON ANISOTROPY IN THE VELOCITY SPACE

In order to explore the degree of anisotropy of electrons inside a minimum-B trapped ECR-based plasma, we made use of the numerical code described above, to simulate an argon plasma, sustained by microwaves at 12.84 GHz, and 400 W of power. The plasma confinement is supported by a specific magnetostatic minimum-B field profile, having at this frequency a ratio of $B_{min}/B_{ECR} = 0.87$. Only electrons (100 000 particles) have been followed in the numerical simulations, and 3D density and energy density maps were produced. After a simulation time of 250 μs, and one self-consistent simulation loop, the electrons still present in the chamber are around 15 000. Figure 1 shows the distribution

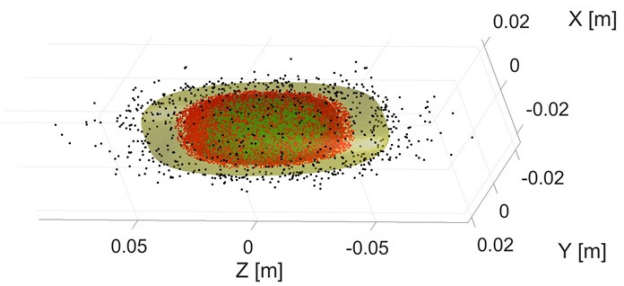

Figure 1: Distribution of electrons in chamber, close to isomagnetic isosurfaces at: $B < 0.96\,B_{ECR}$ (green dots), $B > 1.2\,B_{ECR}$ (black dots - yellow isosurface), and $0.96\,B_{ECR} < B < 1.04\,B_{ECR}$ (red dots - red isosurface).

of bunch of these particles located around three nested and closed isomagnetic surfaces: among the three, the densest one refers to the volume around the isosurface at $B = B_{ECR}$ (red). Here, it is expected the best wave-to-particle coupling and resonant electron's heating. At higher (lower) B-field isosurfaces, particles distribute in the so-called rarefied halo (denser plasmoid) volume. For each spatial region, the transverse $v_\perp$, and longitudinal $v_\parallel$, component of particles' velocity with respect to the magnetic field, has been calculated. Each particle then can be located in the velocity space by a set of coordinates $(v_\parallel, v_\perp)$.

Figure 2 (top-panels) shows a contour plot of the local distribution of particles in the velocity space ($v_\perp$ vs. $v_\parallel$) in the three selected regions. The color refers to the amount of particles with a given $(v_\parallel, v_\perp)$. Figure 2 (bottom-panels) shows the same information, but plotted in terms of $\frac{v_\perp}{|v|}$ and $\frac{v_\parallel}{|v|}$ space, with $|v| = \sqrt{v_\perp^2 + v_\parallel^2}$. The figures provide a set of relevant information: first, there is a different spread of velocity anisotropy in the velocity space which has an evident spatial dependency, and shows a tendency of particles distributing at $v_\perp > v_\parallel$. Second, particles close to the plasmoid show a trend towards a mean isotropic distribution, whereas particles close especially to the ECR surface show a general anisotropic behavior. The halo region has only some particular spot away from the isotropic line. Finally, a *quantitative* idea of the most anisotropic velocity distribution can be appreciated from Figs. 2(d-f), where the ratio $v_\perp/v_\parallel$ in the plasmoid (d) does not go beyond $2 \div 4$. Conversely, the same ratio in the ECR region (f) reaches values even larger than 10. The results promisingly fulfill the experimental/theoretical expectations concerning highly anisotropic electrons, usually located at the ECR surface. On the other side, less anisotropic electrons which are expected lying inside the inner regions of the plasmoid, are evidenced as well by the numerical simulations. Moreover, the simulation parameters (RF Power $P = 400$ W, and $B_{min}/B_{ECR} = 0.87$), characterize a plasma which in the literature is usually referred to as *unstable*, and to be prone to kinetic instabilities [11]. These kind of plasma features are mostly related to strongly anisotropic electrons with a ratio of $v_\perp/v_\parallel \gg 1$ [12], and this aspect has been highlighted by all the spatial regions explored, where generally $v_\perp \geq v_\parallel$.

SPACE-DEPENDENT ELECTRON ENERGY DISTRIBUTION FUNCTION FOR ECR-BASED PLASMA

A study of ECR-based plasma's EEDF has been based on the need to make progress in the space-dependent plasma electron properties characterization, on which several mechanisms and phenomena interesting for ECRIS devices and ECRIS-based technologies depend. It is of fundamental importance to obtain a space-resolved information on the electron energy distribution especially because of the already mentioned ECR plasma features, i.e., high inhomogeneity and strong anisotropy.

Here we present a step-by-step determination of suitable analytic EEDFs that can effectively describe space-dependent properties of minimum-B ECRIS plasma electron populations. The study is based on two main steps. First, we have simulated the same argon ECRIS plasma with same magnetostatic structure, with pumping microwave field frequency at 12.84 GHz, and 30 W of power. The numerical

ISBN: 978-3-95450-226-4 ISSN: 2222-5692 doi:10.18429/JACoW-ECRIS2020-TUYZO01

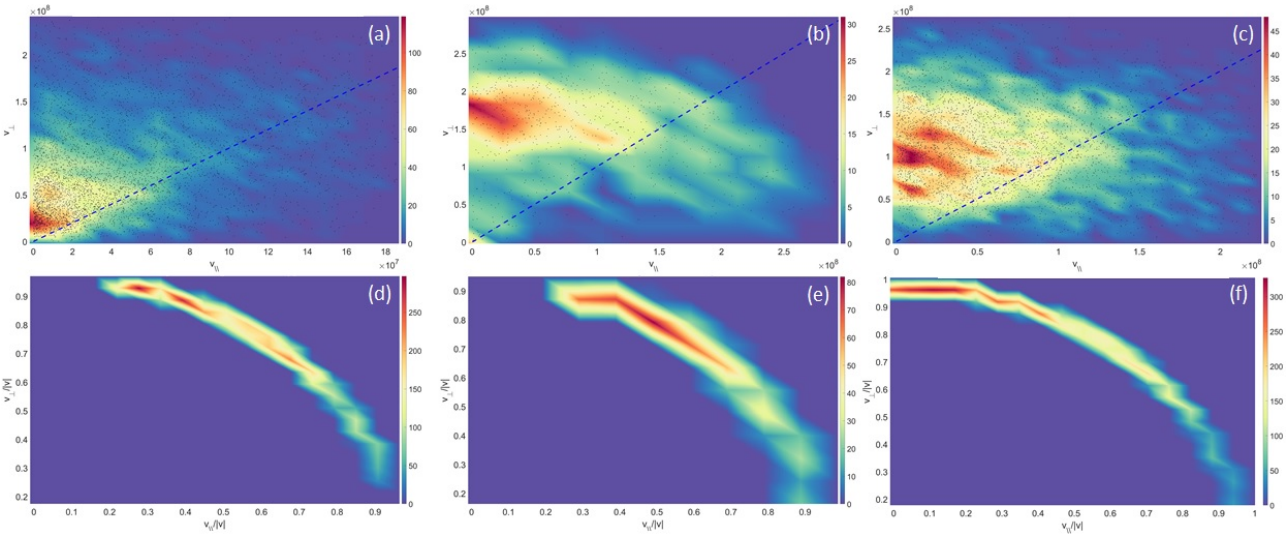

Figure 2: (**Top-panels**) Local distribution of particles in the velocity space ($v_{\parallel}$,$v_{\perp}$) for both particles at the (a) plasmoid, (b) halo, and (c) ECR isomagnetic surfaces. The isotropic line ($v_{\parallel} = v_{\perp}$) is shown (dashed line). (**Bottom-panels**) Same as in the top panels: (d) plasmoid, (e) halo, and (f) ECR region, but in terms of ($\frac{v_{\perp}}{|v|}$, $\frac{v_{\parallel}}{|v|}$).

simulations were settled up to provide 3D density, ρ_i, and energy density, E_i, maps, sliced into seven electron energy intervals, i.e., [0-2] keV, [2-4] keV, ..., [12-∞] keV. Second, based on this first slicing, an average electron energy-based $\langle E\rangle = \sum_{i=1}^{7} \rho_i E_i / \sum_{i=1}^{7} \rho_i$ selection of region of interest (ROI) in the simulation domain has been performed. This consists in grouping cells of the simulation domain whose $\langle E\rangle$ content belongs to the same defined range. Figure 3 shows some isosurfaces of few of these ROIs inside the plasma chamber, where higher $\langle E\rangle$-based ROIs distribute deeper inside the plasmoid region, in a shell-structure shape. Therefore, we have evaluated ROI-averaged electron density

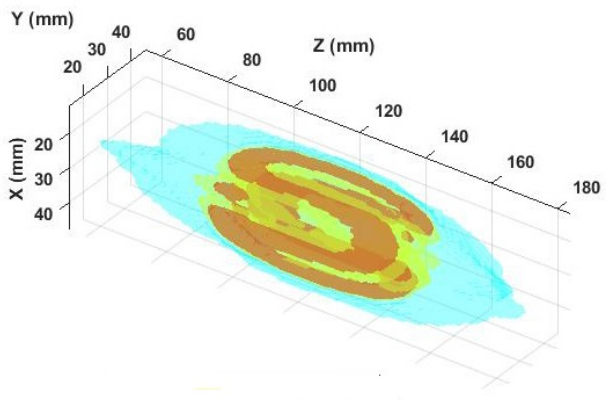

Figure 3: Structure and position in the space of $\langle E\rangle$-based ROIs: $\langle E\rangle \in [0-0.1]$ keV (ROI1, cyan), $\langle E\rangle \in [0.2-0.3]$ keV (ROI3, yellow), $\langle E\rangle \in [0.3-0.4]$ keV (ROI4, red).

and energy density for all the seven energy intervals, with the idea to generate collective data for each ROI, starting from the energy density and density maps produced by the numerical simulation. Next, we have compared the calculated data for each ROI to estimated density and energy density by using 2- and 3-components EEDFs. The nature of plasma properties has suggested a peculiar non-Maxwellian energy distribution, as well as electrons which distribute in two to three populations depending on their energy content. The EEDFs considered in our survey have been constructed as an adequate combination of low- and mid-energy Maxwellian function f_M

$$f_M(E;k_BT_e) = \frac{2}{\sqrt{\pi}} \frac{\sqrt{E}}{(\sqrt{k_BT_e})^3} e^{-\frac{E}{k_BT_e}}, \qquad (1)$$

where T_e is the electron temperature, and k_B is the Boltzmann constant, and functions capturing the high-energy population. The high-energy tails have been described both using Maxwellian or a Druyvesteyn function f_D

$$f_D(E;k_BT_e) = 1.04 \frac{2}{\sqrt{\pi}} \frac{\sqrt{E}}{(\sqrt{k_BT_e})^3} e^{-0.55\frac{E^2}{(k_BT_e)^2}}. \qquad (2)$$

This latter has been considered in the literature as a more accurate function describing high-energy electrons which for some reasons do not thermalize. With this in mind, we have performed this *qualitative* comparison, where estimates of density $(\rho_{ij})_{est}$, and energy density $(E_{ij})_{est}$ are obtained through the several test EEDFs, according to Eqs. (3)

$$(\rho_{ij})_{est} = (\sum_{i=1}^{7} \rho_{ij}) \int_{E_{min}}^{E_{max}} f(E;(k_BT_l)_j;\ldots;(k_BT_h)_j)\mathrm{d}E$$
$$(E_{ij})_{est} = \frac{\int_{E_{min}}^{E_{max}} f(E;(k_BT_l)_j;\ldots;(k_BT_h)_j)E\mathrm{d}E}{\int_{E_{min}}^{E_{max}} f(E;(k_BT_l)_j;\ldots;(k_BT_h)_j)\mathrm{d}E}, \qquad (3)$$

ISBN: 978-3-95450-226-4 ISSN: 2222-5692 doi:10.18429/JACoW-ECRIS2020-TUYZO01

where i and j are the energy intervals and ROI indices, respectively. Also a *quantitative* analysis has been performed cell-by-cell about the goodness of fit parameters, and then of the EEDF, in each of the ROIs, by computing the *mean squared error* (MSE) and the correlation r^2-score coefficient for each EEDF. The function minimizing the MSE value, and maximizing r^2, in all the ROIs has been considered as the most suitable in describing this kind of plasma. Figure 4 shows results for the MSE and r^2 for the EEDFs consid-ered. The best fitting function in all the ROIs is EEDF2, i.e., that one composed by a low-energy Maxwellian and a high-energy Druyvesteyn function. Figure 4 also shows that simulated data are appreciably well approximated by the EEDF2, numerically validating the local information on the electron energy distribution.

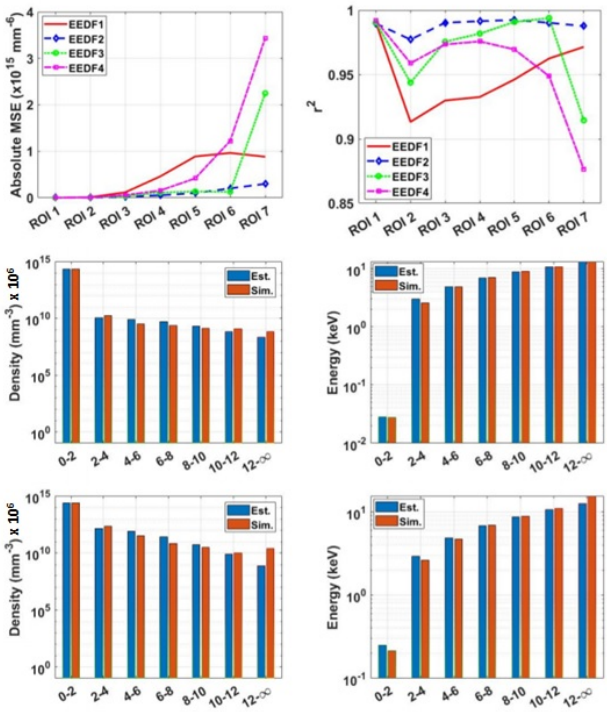

Figure 4: (**Top**). MSE (left) and r^2 (right) score for 4 different EEDFs used to fit data in each of the ROIs. (**Mid**). ROI1 density (left) and energy density (right) simulated data contrasted to the EEDF2 estimated counterparts, according to Eqs. (3). (**Bottom**). ROI3 density (left) and energy density (right) simulated data contrasted to the EEDF2 estimated counterparts.

VALIDATION OF THE CONTINUOUS EEDF

In order to validate the analytic EEDF obtained, we have used it for numerical estimates to be compared with experimental observations and theoretical predictions. One first test bench was provided by the intention to provide a theoretical support to a space-resolved X-ray spectroscopy experiment using quasi-optical methods looking to the fluorescence X-ray emission from K-shells of Ar plasma, conducted jointly by the ATOMKI, Debrecen and the INFN-LNS teams, as a plasma diagnostics tool [13]. The EEDF and simulated density for each individual plasma cell were used to calculate a 3D space-resolved Kα emission rate map. By simulating also the geometrical efficiency of the detector, and other quantities of interest like the quantum efficiency of the CCD camera, as well as the plasma exposure time, the final emission map was obtained. This was compared with the experimental results. Figure 5 shows the results. While the photon counts are not perfectly matching, aspect requiring further analyses, the estimates can be considered close enough in describing the physical experimental imaging. A second test bench for the EEDF validation regarded

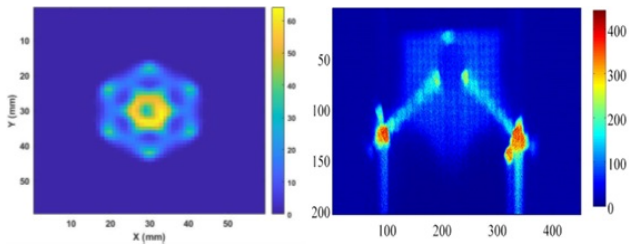

Figure 5: (**Left**) Longitudinally-integrated estimated K-α map at the CCD camera, considering total emission, local geometrical and quantum efficiency. (**Right**) Experimental photon counted images, from Ref. [13].

a first evaluation of the ion CSD for a specific ROI, starting from ROI-averaged plasma density and EEDF inputs. The ion CSD was calculated using the code-suite FLYCHK [14] which required the above mentioned input data as control parameters. Since the code is essentially 0D, each ROI was treated as a single cell, and the collective data generated for the ROI was taken as the spatially-aggregated electron data for that cell. The CSD calculations were performed for Ar ions. Figure 6 displays ROI 1 and 4, together with the extracted collective CSD of Ar ions. It can be seen that the higher the energy of the electrons,the higher the charge states of the ion CSD peak, which is perfectly consistent with expectations.

CONCLUSION

In the present work, we have presented preliminary results obtained from numerical tools developed to explore space-dependent electron properties and structure. Special attention has been devoted to the study of the ECRIS-based plasma electron anisotropy in the velocity space, which is of fundamental relevance in the study of plasma kinetic instabilities, and related transient electromagnetic emissions. A numerical routine has been developed to spatially resolve the electrons velocity distribution, and first promising results have been shown. Experimental evidence of much anisotropic behavior close to the ECR surface, as well as from its inner region, where x-ray burst have been observed [15, 16], have been also captured by the numerical results. Furthermore, a detailed study of a space-resolved EEDF has

ISBN: 978-3-95450-226-4 ISSN: 2222-5692 doi:10.18429/JACoW-ECRIS2020-TUYZO01

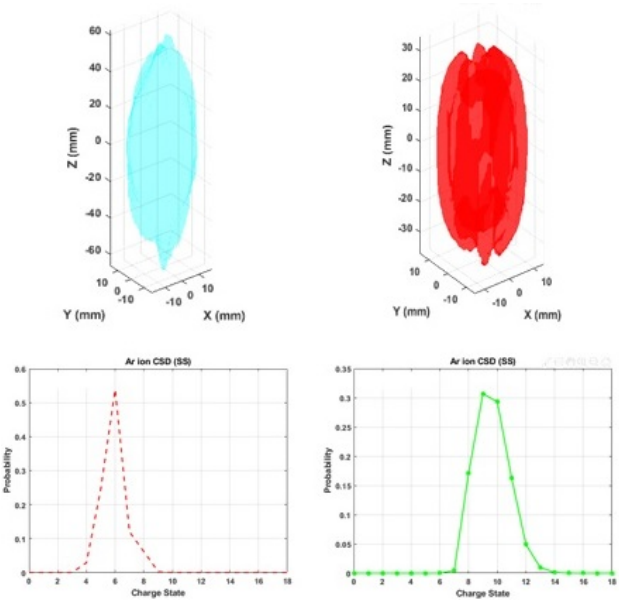

Figure 6: Ion CSD for collective electron data in ROI1 (left) and ROI4 (right) resulting as from FLYCHK code.

been carried out, with preliminary evaluation of analytic EEDF describing the electron properties in a minimum-B ECRIS plasma. The resulting function has been used to contrast experimental results from x-ray spectroscopy and imaging of K-α emission [13], with numerical estimates of the same. The comparison has shown sufficiently good approximation of the experimental results, which require further improvements. The same EEDF has been used for a first evaluation of Ar ion CSD in different regions of interest of the plasma, where the electron density and energy content vary. The resulting CSD shows such spatial dependency, with expected shift of the CSD to higher charge states upon increasing the energy of electrons. This latter result opens to future perspectives, among which, a possible introduction of the space-resolved 0D information on the CSD into the 3D self-consistent machinery, to introduce ion-electron collisional effects with a spatial dependency, and explore this influence on the ECRIS performances. Finally, the same becomes of great relevance - beyond ECRIS purposes - in the Nuclear and AstroNuclear Physics, for studying stellar enhanced nuclear phenomena in plasma, where a certain ion CSD and atomic level population impact on the nuclei's decay mechanisms. The INFN's PANDORA [17] project plans to use these data on ECRIS plasmas for its survey on such phenomena.

ACKNOWLEDGEMENTS

The authors wish to thank the 3rd Nat. Comm. of INFN, under the PANDORA_Gr3 Grant, for the financial support. The authors wish to thank also Dr. Richard Ràcz from ATOMKI - Institute of Nuclear Science (Debrecen, HU) for valuable support in the Kα emission rate evaluation and comparison to experimental results.

REFERENCES

[1] R. Geller, *Electron cyclotron resonance ion sources and ECR plasmas*. Bristol, UK: IOP Publishing, 1996.

[2] I. Izotov *et al.*, "Broadband microwave emission spectrum associated with kinetic instabilities in minimum-B ECR plasmas," *Phys. Plasma*, vol. 24, p. 043515, Apr. 2017. https://doi.org/10.1063/1.4981387

[3] R. A. Treumann, "The electron cyclotron maser for astrophysical application," *Astron. Astrophys. Rev.*, vol. 13, pp. 229-315, Jul. 2006. doi.org/10.1007/s00159-006-0001-y

[4] A. G. Shalashov *et al.*, "Maser based on cyclotron resonance in a decaying plasma," *JETP Lett.*, vol. 84, pp. 314-319, Nov. 2006. doi.org/10.1134/S0021364006180081

[5] O. Tarvainen *et al.*, "Beam current oscillations driven by cyclotron instabilities in a minimum-B electron cyclotron resonance ion source plasma," *Plasma Sources Sci. Technol.*, vol. 23, no. 2, Apr. 2014. doi.org/10.1088/0963-0252/23/2/025020

[6] D. Mascali *et al.*, "3D-full wave and kinetics numerical modelling of electron cyclotron resonance ion sources plasma: steps towards self-consistency," *Eur. Phys. J. D*, vol. 69, p. 27, Jan. 2015. doi.org/10.1140/epjd/e2014-50168-5

[7] G. Torrisi *et al.*, "Full-wave FEM simulations of electromagnetic waves in strongly magnetized non-homogeneous plasma," *Journal of Electromagnetic Waves and Applications*, vol. 28, p. 9, Apr. 2014. doi.org/10.1080/09205071.2014.905245

[8] C. S. Gallo *et al.*, "Self-consistent electromagnetic analysis of the microwave-coupling of an electron cyclotron resonance-based charge breeder," *Rev. Sci. Instrum.*, vol. 91, p. 033501, Feb. 2020. doi.org/10.1063/1.5129622

[9] A. Galatà *et al.*, "A new numerical description of the interaction of an ion beam with a magnetized plasma in an ECR-based charge breeding device," *Plasma Sources Sci. Technol.*, vol. 25, p. 045007, Jun. 2016. doi.org/10.1088/0963-0252/25/4/045007

[10] O. Tarvainen *et al.*, "Diagnostics of a charge breeder electron cyclotron resonance ion source helium plasma with the injection of $^{23}Na^{1+}$ ions," *Phys. Rev. Accel. Beams*, vol. 19, p. 053402, May 2016. doi.org/10.1103/PhysRevAccelBeams.19.053402

[11] V. Skalyga *et al.*, "Kinetic instabilities in a mirror-confined plasma sustained by high-power microwave radiation," *Phys. Plasma*, vol. 22, p. 083509, 2015. doi.org/10.1063/1.4978565

[12] A. G. Shalashov *et al.*, "Kinetic instabilities in a mirror-confined plasma sustained by high-power microwave radiation," *Phys. Plasma*, vol. 24, p. 032111, Mar. 2017. doi.org/10.1063/1.4978565

[13] R. Ràcz *et al.*, "Electron cyclotron resonance ion source plasma characterization by energy dispersive x-ray imaging," *Plasma Sources Sci. Technol.*, vol. 26, p. 075011, Jul. 2017. doi.org/10.1088/1361-6595/aa758f

[14] H.-K. Chung *et al.*, "FLYCHK: Generalized population kinetics and spectral model for rapid spectroscopic analysis for all elements," *High Energy Density Phys.*, vol. 1, no. 1, pp. 3-12, Dec. 2005. doi.org/10.1016/j.hedp.2005.07.001

ISBN: 978-3-95450-226-4 ISSN: 2222-5692 doi:10.18429/JACoW-ECRIS2020-TUYZO01

[15] V. Skalyga *et al.*, "Microwave emission from ECR plasmas under conditions of two-frequency heating induced by kinetic instabilities," *AIP Conference Proceedings (2011)*, p. 020015, Sep. 2018. doi.org/10.1063/1.5053257

[16] E. Naselli *et al.*, "Impact of two-close-frequency heating on ECR ion source plasma radio emission and stability," *Plasma Sources Sci. Technol.*, vol. 28, p. 085021, Aug. 2019. doi.org/10.1088/1361-6595/ab32f9

[17] D. Mascali *et al.*, "PANDORA, a new facility for interdisciplinary in-plasma physics," *Eur. Phys. J. A*, vol. 53, p. 145, Jul. 2017. doi.org/10.1140/epja/i2017-12335-1